

Size effects in the mechanical behavior of cellular materials

C. TEKOGU*, P. R. ONCK

Micromechanics of Materials, Materials Science Center, University of Groningen, 9747 AG Groningen, The Netherlands

E-mail: c.tekoglu@rug.nl

E-mail: p.r.onck@rug.nl

Effective mechanical properties of cellular materials depend strongly on the specimen size to the cell size ratio. Experimental studies performed on aluminium foams show that under uniaxial compression, the stiffness of these materials falls below the corresponding bulk value, when the ratio of the specimen size to the cell size is small. Conversely, in the case of simple shear and indentation, the overall stiffness rises above the bulk value. Classical continuum theory, lacking a length scale, cannot explain this size dependent mechanical behaviour. One way to account for these size effects is to explicitly model the discrete cellular morphology. We performed shear, compression and bending tests using discrete models, for hexagonal (regular and irregular) microstructures. Even though discrete models give a very good agreement with the experiments, they are computationally expensive for complex microstructures, especially in three dimensions. To overcome this, one can use a generalized continuum theory, such as Cosserat continuum theory, which incorporates a material length scale. We fit the Cosserat elastic constants of the models by comparing the discrete calculations with the analytical Cosserat continuum solutions in terms of macroscopic properties. We critically address the limitations of the Cosserat continuum theory. © 2005 Springer Science + Business Media, Inc.

1. Introduction

Natural materials such as wood, cork or cancellous bone, and man-made materials, such as metal honeycombs and foams, are well-known examples of cellular solids. Common to all of them is a microstructure consisting of an interconnected network of struts or plates. The high specific bending stiffness is an important property, which, among other multifunctional features, has made metal foams a competitive engineering material in the last decade. They are often used in sandwich panels, where they are laminated between two dense solids to increase the moment of inertia with a minimum increase in weight. Another important application of polymer and metal foams is in energy absorption devices, from simple coffee cups to energy collection systems on satellites. They are also widely used in packaging of materials. Nevertheless, despite the extensive use of foams in industry, a better understanding of their mechanical properties is required.

Compression of aluminum foams shows that the Young's modulus is lower for specimens with a lower ratio of specimen size to cell size [1]. This size effect is caused by weak boundary layers related to the reduced constraint at the free surfaces [2]. Shear tests

on sandwich panels, on the other hand, show that the shear strength is higher for lower specimen size, relative to the cell size [1, 3]. The strengthening under shear for smaller specimens is explained by the existence of a constrained layer at the top and at the bottom boundaries, where the foam is bound to the face sheets.

Classical continuum theory, which does not incorporate a length scale, cannot capture these size effects. One way to overcome this problem is to take into account the discreteness of the microstructure by modeling each cell wall as a beam element. This method correlates well with experiment, but is computationally expensive for complex microstructures. Another approach is to use a generalized (enhanced) continuum theory. One of the simplest generalized continuum theories is the Cosserat theory, where rotations are introduced as independent degrees of freedom. As a result, the interaction between two neighboring material points does not occur only via forces, but also via moments. This requires additional constants in the constitutive equations, relating couple stresses (stresses due to moments) to curvatures (derivatives of rotations), which are hard to determine experimentally.

*Author to whom all correspondence should be addressed.

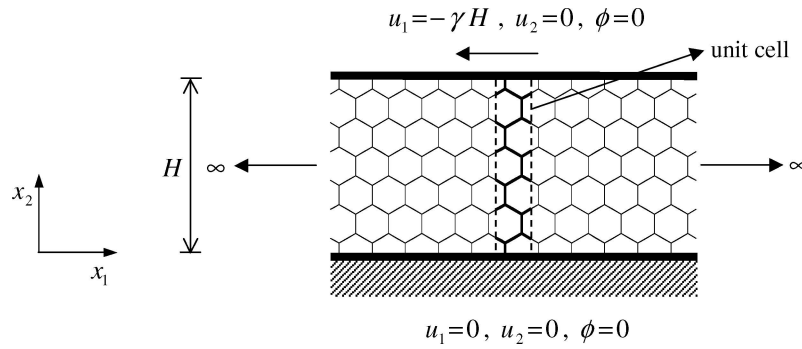


Figure 1 The boundary value problem for simple shear of a specimen with a regular hexagonal microstructure in the default orientation.

In this paper, our aim is to obtain the Cosserat elastic constants of a two-dimensional cellular solid. We solve simple shear, uniaxial compression and pure bending boundary value problems, first by performing finite element analyses on the discrete models and then analytically by using the Cosserat continuum theory. We fit the elastic constants of the material by comparing the two solutions of the simple shear problem in terms of the best agreement in the macroscopic shear modulus. Finally, we check whether these constants give meaningful results for uniaxial compression and bending.

2. Discrete calculations

The primary deformation mechanism of open-cell (and closed-cell metal) foams is bending of the cell walls. Since hexagons are isotropic and have bending as principal deformation mechanism, they form a good 2D model material for real foams.

In this section, we will perform simple shear, uniaxial compression and pure bending tests. We use both regular and perturbed hexagons to represent the microstructure of metal foams.

2.1. Simple shear

Fig. 1 shows the boundary conditions corresponding to a shear test on a sandwich panel having a regular hexagonal microstructure as a core. We model each cell wall by Timoshenko beam elements, using the commercial finite element package ABAQUS. The cell walls are assumed to have a uniform thickness, t , throughout the whole material. To avoid edge effects common to the shear problem, we take an infinitely long material in the x_1 direction. Consequently, it suffices to analyze only one column of cells and to apply periodic boundary conditions on both sides of the unit cell (see the indicated region in Fig. 1).

The macroscopic shear stress is obtained by dividing the sum of the reaction force(s) at the top node(s), F , by the surface area of the unit cell, $\sqrt{3}lb$, where b is the out of plane thickness and l is the cell wall length. The ratio of the shear stress to the applied shear strain gives the macroscopic shear stiffness, $F/(\sqrt{3}l\gamma)$.

The value of the macroscopic shear stiffness depends not only on the relative specimen height H/d (d is the cell size), but also on the length and the orientation of the cell walls at the boundaries, to which we refer

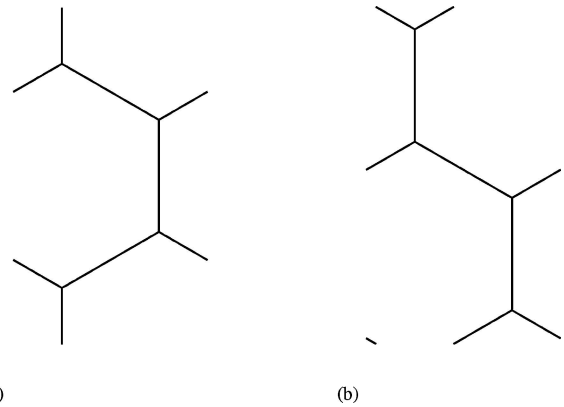


Figure 2 Two different cuts with the same height, for the regular hexagonal microstructure in the default orientation.

to as the boundary configuration in the following. We analyze two different orientations of the hexagonal microstructure with respect to the loading direction. The first one is referred to as the default orientation (see Fig. 1), and the one rotated at 90 degrees as the rotated orientation. To consistently check the dependence on the boundary configuration, for each value of H/d we analyze all possibilities of “cutting” the “specimen” from the hexagonal structure. Fig. 2 shows two different cuts in the default orientation, with the same relative height, but with different boundary configurations. In the case of regular hexagons, only a few cuts (6 in the case of the default orientation and 8 for the rotated orientation) are enough to cover almost all possible boundary configurations. To have a common measure for the cell size d for both orientations we take $d \approx 1.82l$, equal to the diameter of a circle with the same area as a regular hexagonal cell with a cell wall length l .

Fig. 3a and b show the macroscopic shear stiffness, $F/(\sqrt{3}l\gamma)$, normalized by the shear modulus, G , plotted against the relative specimen size, H/d , for the default and the rotated orientations, respectively. The shear modulus G is the effective shear modulus of an infinitely large block with the same microstructure. For regular hexagonal microstructures, irrespective of the cell orientation, the shear modulus is given by:

$$G = \frac{1}{\sqrt{3}} E_s (t/l)^3 \frac{1}{1 + (3.30 + 1.75\nu_s)(t/l)^2}, \quad (1)$$

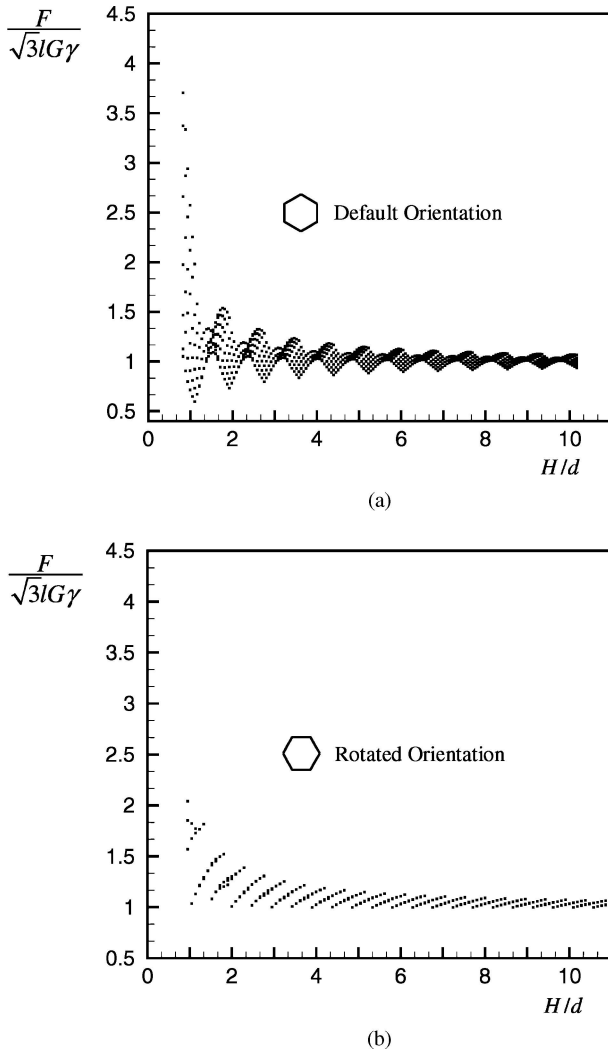


Figure 3 $F/(\sqrt{3}lG\gamma)$ plotted against H/d for the regular hexagonal microstructure: (a) In the default orientation (6 cuts per H/d). (b) In the rotated orientation (8 cuts per H/d).

where E_s is the Young's modulus and ν_s is the Poisson's ratio of the solid material that the specimen is made of [4]. The density of the specimens is kept constant by changing the uniform cell wall thickness accordingly.

Fig. 3a shows that there is a large scatter in data, especially in the small H/d regime, which decreases with increasing height. The overall shear stiffness increases with decreasing height, and it converges to the shear modulus with increasing H/d . This strengthening behavior, $F/(\sqrt{3}lG\gamma) > 1$, is associated with the constrained rotations of the cell walls bound to the face sheets. It is interesting to see that softening, i.e. $F/(\sqrt{3}lG\gamma) < 1$, is also possible for some boundary configurations. This is the case for cuts with a smaller cell wall thickness, related to the fact that we keep the density constant.

In Fig. 3b, we see that no softening occurs, meaning that the effect of the constrained boundary layer (leading to strengthening) is always dominant over the effect of the lower cell wall thickness (leading to softening). On average, we observe a strengthening behavior in the small H/d regime for both orientations. The normalized macroscopic shear stiffness, $F/(\sqrt{3}lG\gamma)$, converges to

1 with increasing height, as would be expected.

The two orientations that we study here are two extreme cases for the regular hexagonal microstructures, where for the default orientation one of the three "close-packed crystal" orientations is parallel to the face sheets, while in the rotated orientation it is perpendicular to it. To cover the complete range of boundary configurations for the hexagonal structure, one would have to consistently check all intermediate orientations, and for each orientation analyze all possible cuts corresponding to a single H/d value. For orientations inbetween the default and rotated, a range of boundary configurations is present in each boundary value problem, giving rise to properties that are likely to lay inbetween the properties of the two extreme orientations.

Despite their utility for understanding some of the key aspects in the mechanical behavior of cellular solids (especially analytically), regular hexagons do not represent realistically the stochastic nature of foams. The regular hexagonal microstructure has a very elongated yield surface, indicating a high hydrostatic strength. Real foams, however, have an approximately circular yield surface, with a hydrostatic yield strength almost equal to their compressive yield strength [5, 6]. The primary deformation mechanism for the regular hexagonal microstructure under uniaxial loading is bending of the cell walls, where it is stretching under biaxial loading. Chen and coworkers [7] showed that imperfections such as cell wall misalignments change the deformation mechanism under biaxial loading to bending, causing a knockdown in the hydrostatic properties, leading to a circular yield surface. We introduce cell wall misalignments into the regular hexagonal structures by displacing all junctions in the structure in a random direction and a random distance chosen from a uniform distribution (0, 0.4l). Due to the stochastic imperfections, the unit cell is enlarged to $L = 150d$, still featuring periodic boundary conditions (see Fig. 4). Even though the perturbed hexagons are produced in a random manner, the structure still features the "close-packed crystal" orientations of the regular hexagonal structures.

To capture all boundary configurations for a single H/d value for the perturbed microstructures, we take 100 different cuts of a big block for each H/d . By performing convergence tests for $H/d = 1, 2, 3$ and 5 we found that for more than 100 cuts, the average and the standard deviation of the macroscopic shear stiffness did not change anymore. Fig. 5a and b show $F/(LG\gamma)$ plotted against H/d , for the default and the rotated orientations, respectively. Note that here G is the shear modulus of an infinitely large block with the same microstructure. We see that there is no softening behavior for any boundary configuration, in either case. We detect a strengthening in the small H/d regime in both cases, being slightly more pronounced in the default orientation. The scatter in data for small H/d is larger in the default orientation and tends to zero with increasing height, while the value of the macroscopic shear stiffness converges to the classical value. The strengthening effect is larger than for the regular hexagons (compare with Fig. 3).

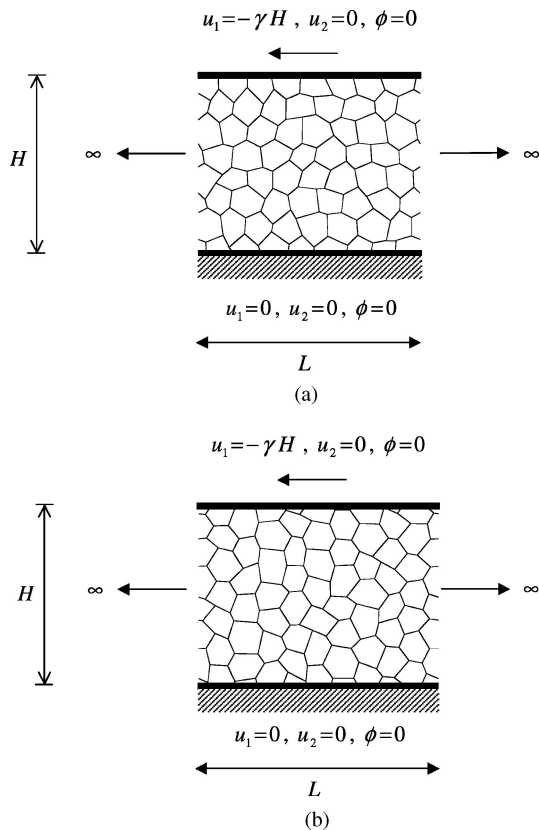
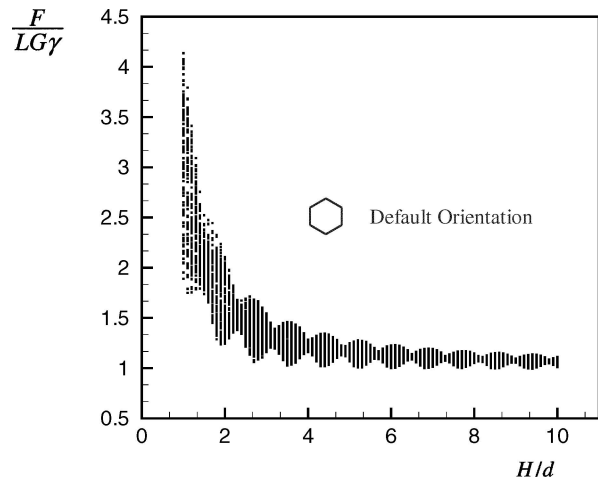


Figure 4 Simple shear of the perturbed hexagonal microstructure: (a) In the default orientation. (b) In the rotated orientation.

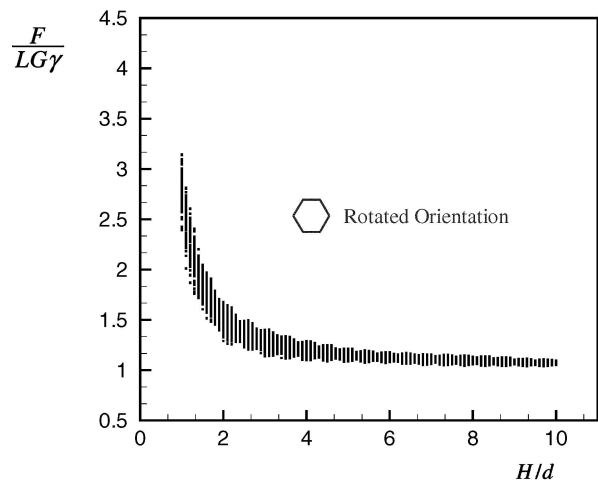
2.2. Uniaxial compression

Fig. 6 shows the boundary conditions for a uniaxial compression test in the x_1 direction (rotated orientation) of an aluminum foam with a perturbed hexagonal microstructure. We apply periodic boundary conditions on the left and the right boundaries of the structure, to imitate an infinitely long material in the x_1 direction: $u_\alpha^J - u_\alpha^I = \varepsilon_{\alpha\beta}(x_\beta^J - x_\beta^I)$ and $\phi^J - \phi^I = 0$, ($\alpha, \beta = 1, 2$), where ϕ is the rotation of the cell walls in the x_1 - x_2 plane. I and J are pairs of nodes on opposite edges of the mesh (see Fig. 6) and $\varepsilon_{12} = \varepsilon_{22} = 0$. The compressive stress is calculated by dividing the sum of the reaction forces on the boundary nodes by the area under compression, Hb . The uniaxial compressive stiffness is calculated from the ratio of the compressive stress and the compressive strain, and is given by $F/(H\varepsilon_{11})$. The length of the specimens relative to the cell size is taken to be large enough ($L/d = 150$) to ensure that the uniaxial compressive stiffness is independent of L/d . We increase the height of the block, taking 100 different cuts per a single H/d value.

Fig. 7a and b show the calculated uniaxial compressive stiffness, $F/(H\varepsilon_{11})$, normalized by the Young's modulus E , plotted against H/d , for the default and the rotated orientations, respectively. The Young's modulus E is the Young's modulus of an infinitely large block with the same microstructure. We detect a severe softening in the small H/d regime, for both of the orientations, with the scatter being much larger for the rotated orientation. In Fig. 6, we see clearly that the cell walls located at the boundaries perpendicular to the direction of compression are stress free. In addition, the



(a)



(b)

Figure 5 $F/(LG\gamma)$ plotted against H/d (100 cuts per H/d) for the perturbed hexagonal microstructure: (a) In the default orientation. (b) In the rotated orientation.

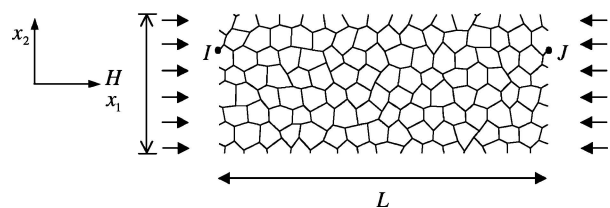
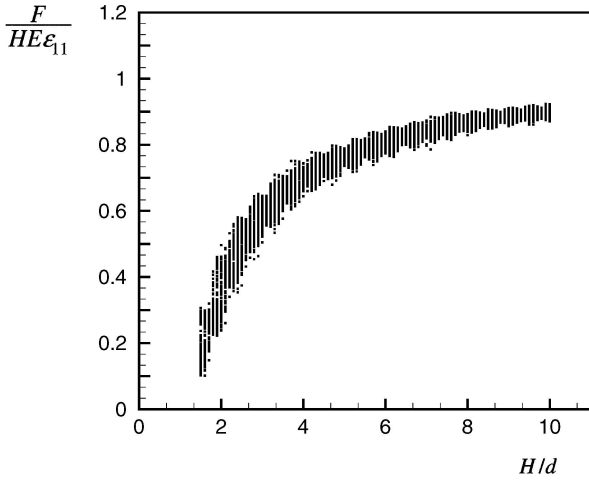
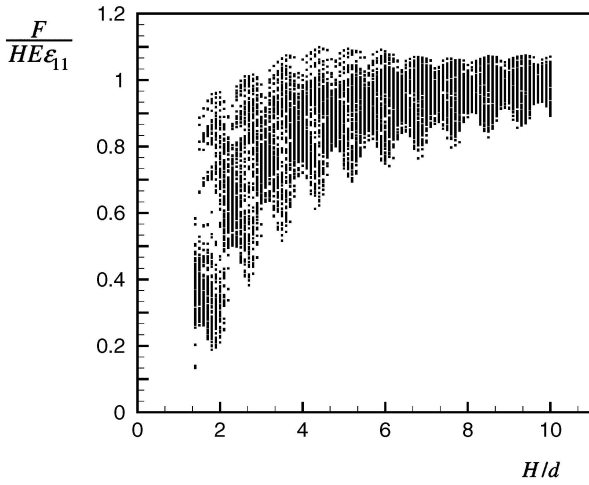


Figure 6 Boundary conditions for a uniaxial compression test of an aluminum foam with a perturbed hexagonal microstructure in the rotated orientation.

cells next to these stress free surface layers are also less constrained than those in the bulk. The area fraction of this weak boundary layer, consisting of both the stress free cell walls and the less-constrained cells, is large when the height of the specimen is small, resulting in a decrease in the macroscopic stiffness [2]. While the specimen size increases, the contribution of this weak boundary layer to the macroscopic stiffness diminishes and the compressive stiffness converges to the classical value. The number of load carrying cell wall members differs from one cut to another for the same height, which is the reason for the scatter in data. The largest possible distance between two subsequent load



(a)



(b)

Figure 7 $F/(HE\varepsilon_{11})$ plotted against H/d (100 cuts per H/d) for the perturbed hexagonal microstructure: (a) In the default orientation. (b) In the rotated orientation.

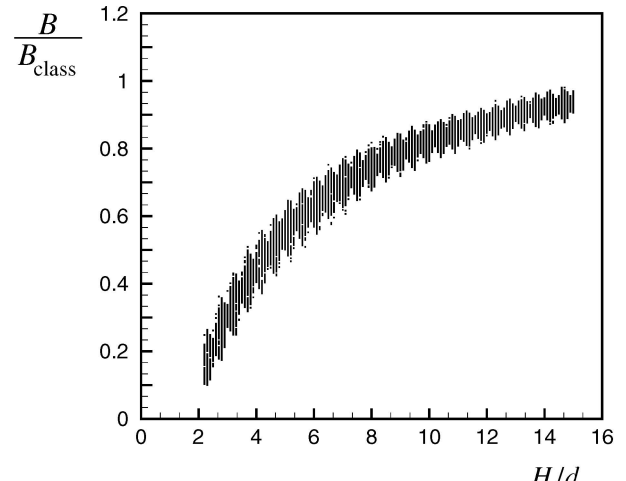
carrying cell edges is larger for the rotated orientation, and therefore the scatter in data is larger as well.

2.3. Pure bending

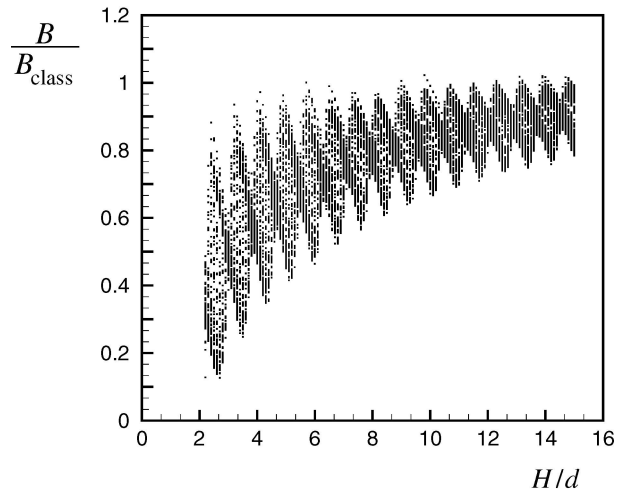
The final boundary value problem that we solve is pure bending of a foam with a perturbed hexagonal microstructure (as in Fig. 6). The displacement and the rotation boundary conditions corresponding to the pure bending boundary value problem are $u_1(x_1 = 0) = 0$, $\phi(x_1 = 0) = 0$, $u_2 = 0$ for one node at $x_1 = 0$ and $u_1(x_1 = L) = -kLx_2$. Here, x_2 is measured from the midsection of the structure and k is the curvature. The macroscopic moment is calculated from the normal forces $f_1^{(k)}$ in the n cell walls at $x_1 = L$ through

$$M = \sum_{k=1}^n f_1^{(k)} x_2^{(k)}. \quad (2)$$

Again, L is taken large enough ($L/d = 150$) to ensure that M is independent of L/d . The bending stiffness B is calculated from M/k . Fig. 8a and b show the normalized macroscopic bending stiffness, B/B_{class} , plotted against H/d , for the default and the rotated orientation respec-



(a)



(b)

Figure 8 B/B_{class} plotted against H/d (100 cuts per H/d) for the perturbed hexagonal microstructure: (a) In the default orientation. (b) In the rotated orientation.

tively. The classical bending stiffness is the bending stiffness of a dense sample with Young's modulus E and height H , defined as $B_{\text{class}} = 1/12EbH^3$. Similar to what we observed in the uniaxial compression test, there is a severe softening in the small H/d regime, and the value of the macroscopic bending rigidity converges to the classical value with increasing height. For a classical material, the material points located at the largest distance from the neutral axis would have the main contribution to the macroscopic bending stiffness. For the cellular microstructure, however, there are stress free boundaries and this causes a softening in the bending rigidity, which is almost entirely due to the softening in the Young's modulus (see Fig. 7). Indeed, the appearance of Fig. 8 is very similar to Fig. 7.

3. Cosserat continuum models

Cosserat continuum theory incorporates rotations as independent degrees of freedom. Therefore, interaction between two neighboring material points can occur via moments as well as via forces. This requires new elastic constants in the constitutive equations of Cosserat materials, relating couple stresses (stresses due to

MECHANICAL BEHAVIOR OF CELLULAR SOLIDS

moments) to curvatures (derivatives of rotations). The coefficients of the elasticity matrix in terms of symmetric (s_{ij} , ε_{ij}) and antisymmetric (τ_{ij} , α_{ij}) components of the stresses and strains for a two dimensional isotropic centrosymmetric Cosserat material reduces to

$$\begin{aligned} s_{11} &= C_{1111}\varepsilon_{11} + C_{1122}\varepsilon_{22}, \\ s_{22} &= C_{1122}\varepsilon_{11} + C_{1111}\varepsilon_{22}, \\ s_{12} &= A_{1212}\varepsilon_{12}, \\ \tau_{12} &= A_{2121}\alpha_{12}, \quad m_{13} = D_{1313}\kappa_{13}, \\ m_{23} &= D_{1313}\kappa_{23}. \end{aligned} \quad (3)$$

For the simple shear problem solved in Section 2.1, the kinematic and equilibrium equations of the Cosserat theory read

$$\begin{aligned} \varepsilon_{11} &= 0, \quad \varepsilon_{22} = 0, \quad \varepsilon_{12} = \frac{1}{2}u_{1,2}, \\ \alpha_{12} &= -\frac{1}{2}(u_{1,2} + 2\phi), \quad k_{13} = 0, \quad k_{23} = \phi_{,2}, \end{aligned} \quad (4)$$

$$s_{12,2} - \tau_{12,2} = 0, \quad m_{23,2} + 2\tau_{12} = 0. \quad (5)$$

Inserting (4) into (5) via the constitutive Equations 3 yields

$$(m + 1)u_{1,2} + 2m\phi_{,2} = 0 \quad (6)$$

$$l_c^2\phi_{,22} - 2m\phi - mu_{1,2} = 0, \quad (7)$$

with

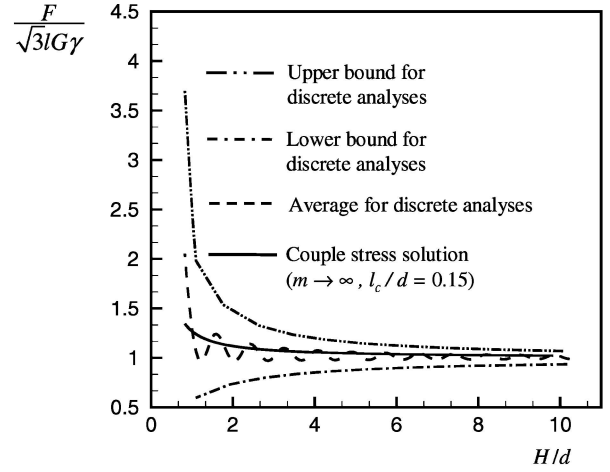
$$m = \frac{A_{2121}}{A_{1212}}, \quad l_c^2 = \frac{D_{1313}}{A_{1212}} \quad (8)$$

The parameter l_c is a material length, and it is often called the characteristic length in the literature. The constant m , on the other hand, is a dimensionless term that can be seen as a coupling factor: the solution converges to the classical solution for $m \rightarrow 0$, and to the couple stress solution for $m \rightarrow \infty$. Couple stress theory, also known as restricted Cosserat theory, is a special case of the Cosserat continuum where the microrotations are equal to the macrorotations, making $\alpha_{12} = 0$ in Equation 4. The complete solution of the differential Equations 6 and 7 is given in [8, 9], from which l_c was identified to set the thickness of the boundary layer as a result of constrained rotations.

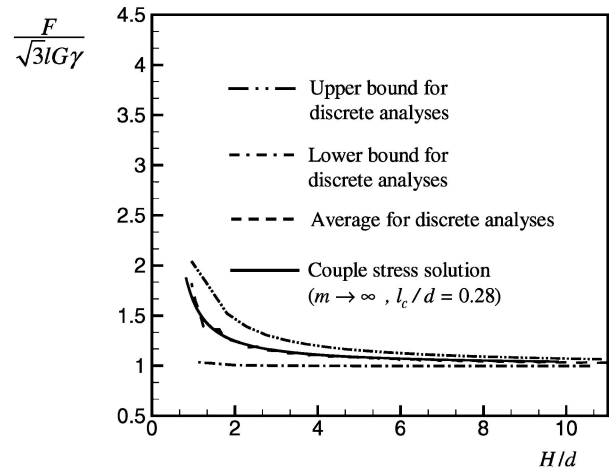
Gauthier and Jahsman [10] have previously solved a pure bending problem of a curved beam made of Cosserat material. Huang and coworkers [11] analyzed a pure bending problem of a straight Cosserat beam. Both studies detect a strengthening in the bending rigidity when the characteristic length l_c is comparable to the beam height. The solution of Huang and coworkers [11], give the bending stiffness of a beam with a height H as

$$B = B_{\text{class}}(1 + 12A_{1212}/C_{1111}(l_c/H)^2). \quad (9)$$

Equation 9 shows that, for large heights, the bending rigidity converges to the classical value, but for heights



(a)



(b)

Figure 9 $F/(\sqrt{3}lG\gamma)$ plotted against H/d for the continuum and discrete solution for the regular hexagonal microstructure: (a) In the default orientation. (b) In the rotated orientation.

of the same order of magnitude as l_c , the bending rigidity is higher than the classical value. Our results for the discrete model, on the other hand, indicate the opposite behavior, giving a lower bending rigidity for small heights.

For uniaxial compression, Cosserat continuum theory does not predict any size effect, due to the absence of rotations and rotation gradients. Therefore, Cosserat solution gives the same result as classical continuum throughout the whole range of length scales.

4. Discussion

In this section, we fit the elastic Cosserat constants of the regular and irregular hexagonal microstructures by comparing the discrete solution for the shear problem with the Cosserat solution, in terms of the best agreement in the macroscopic response. Figs. 9a (10a) and 9b (10b) show the best fit of the Cosserat solution to the average value of the discrete results for the regular (irregular) hexagonal microstructures in the default and the rotated orientations, respectively. To also reflect the scatter, we plot the upper and lower bounds as well. For all cases, the couple stress solution, with $m \rightarrow \infty$, gives the best agreement. We see that the characteristic length l_c depends strongly on the cell orientation in the case of the regular microstructure ($l_c = 0.15d$ for

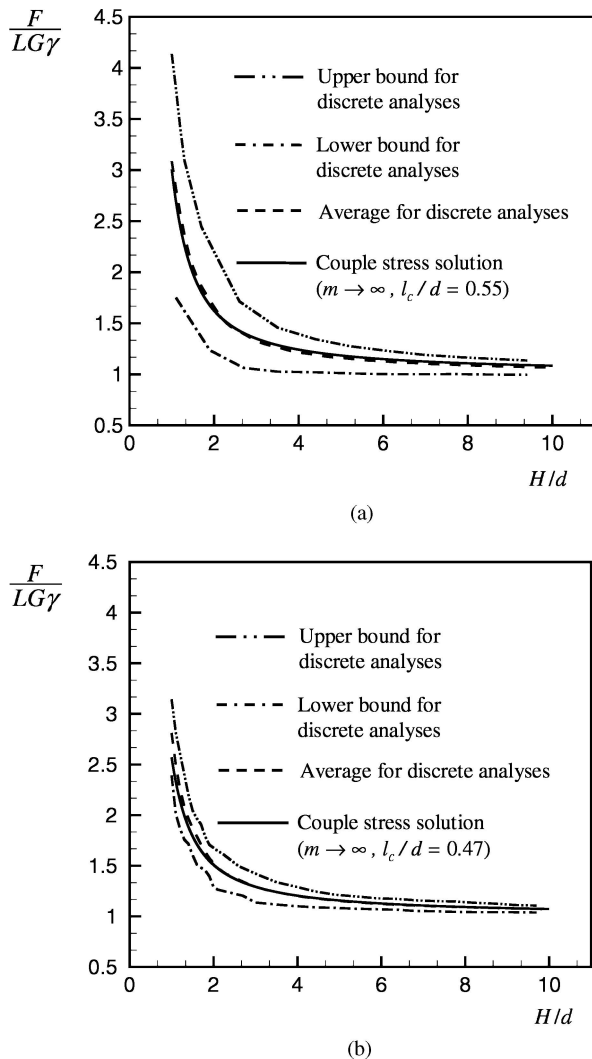


Figure 10 $F/(LG\gamma)$ plotted against H/d for the continuum and discrete solution for the perturbed hexagonal microstructure: (a) In the default orientation. (b) In the rotated orientation.

the default and $l_c = 0.28d$ for the rotated orientations), whereas the difference is very small for the irregular case ($l_c = 0.55d$ versus $l_c = 0.47d$). The strengthening behavior for the irregular hexagonal structure is larger than for the regular structure, which is reflected in a larger value for the characteristic length l_c . Clearly, the characteristic length not only scales with the cell size, it also depends on the cellular morphology.

Hexagonal materials have six-fold symmetry in the x_1 - x_2 plane, which makes them transversely isotropic both in classical and Cosserat continuum theory [12]. This means there is only one l_c value for the regu-

lar hexagonal structure, irrespective of its orientation. This is clearly in contradiction with Fig. 9, yielding two different values for l_c for the default and the rotated orientation. Details with respect to the specific boundary configurations can only be captured in a smeared out, average sense by Cosserat continuum theory. Imperfections in the microstructure already smear out these details, yielding values for l_c that are much closer for the default and the rotated orientations (see Fig. 10). The best that one can do for the hexagonal structures is to take the average of the two extreme orientations analyzed here, yielding $l_c = 0.22d$ for the regular and $l_c = 0.51d$ for the irregular hexagonal microstructures.

For pure bending, the discrete analyses show softening while Cosserat theory shows stiffening. For uniaxial compression, the discrete analyses show softening while Cosserat theory predicts a size independent response. Clearly, free edge effects leading to softening cannot be captured by Cosserat theory. One has to resort to higher order theories that feature additional free surface behavior, as for instance in [13].

References

1. E. W. ANDREWS, G. GIOUX, P. ONCK and L. J. GIBSON, *Int. J. Mech. Sci.* **43** (2001) 701.
2. P. R. ONCK, E. W. ANDREWS and L. J. GIBSON, *Int. J. Mech. Sci.* **43** (2001) 681.
3. C. CHEN and N. A. FLECK, *J. Mech. Phys. Solids* **50** (2002) 955.
4. L. J. GIBSON and M. F. ASHBY, "Cellular Solids" (Cambridge University Press, New York, 1997).
5. G. GIOUX, T. M. MCCORMACK and L. J. GIBSON, *Int. J. Mech. Sci.* **42** (2000) 1097.
6. V. S. DESHPANDE and N. A. FLECK, *J. Mech. Phys. Solids* **48** (2000) 1253.
7. C. CHEN, T. J. LU and N. A. FLECK, *Ibid.* **47** (1999) 2235.
8. S. DIEBELS and H. STEEB, *Proc. Roy. Soc. Lon. Series A* **458** (2002): 2869.
9. C. TEKOGU, P. R. ONCK, Proceedings of the 9th International Conference on the Mechanical Behaviour of Materials (ICM9), Geneva, Switzerland [CD-ROM], (2003).
10. R. D. GAUTHIER and W. E. JASHMAN, *J. Appl. Mech. Trans. ASME* **43** (1976) 502.
11. F. Y. HUANG, B. H. YAN, J. L. YAN and D. U. YANG, *Int. J. Engng. Sci.* **38** (2000) 275.
12. X. L. WANG and W. J. STRONGE, *Proc. R. Soc. Lond. A* (1999) 455,2091.
13. M. E. GURTIN and A. I. MURDOCH, *Arch. Ration. Mech. Anal.* **57** (1975) 291.

Received December 2004
and accepted April 2005